Asian Journal of Chemistry; Vol. 38, No. 4 (2026), 995-1001
ASIAN JOURNAL OF CHEMISTRY
https://doi.org/10.14233/ajchem.2026.35019

Coiled Multiwalled Carbon Nanotubes: Synthesis, Structural Characterisation and Dual Bioactivity against PA-1 Ovarian Cancer Cells and *E. eugeniae*

V. LAKSHMY[1], T. SOMANATHAN[1,*], BINDHU R. KAMATH[1], T. RAJKUMAR[1] and A.R. SASIEEKHUMAR[2]

[1]Department of Chemistry, School of Basic Sciences, Vels Institute of Science Technology and Advanced Studies (VISTAS), Chennai-600117, India
[2]Department of Chemistry, Vinayaka Mission's Kirupananda Variyar Engineering College, Vinayaka Mission's Research Foundation (Deemed to be University), Sankari Main Road, Salem-636308, India

*Corresponding author: E-mail: soma.sbs@vistas.ac.in

Received: 6 October 2025 *Accepted*: 26 February 2026 *Published online*: 8 April 2026 AJC-22320

Coiled multiwalled carbon nanotubes (C-MWCNTs) represent a unique form of carbon nanomaterials, in which the helically stacked structure increases the reactivity, strength and biologically active interactions, thus extending the biologically related application fields compared to straight carbon nanotubes (CNTs). For the synthesis of the C-MWCNTs, this work used the chemical vapour deposition (CVD) method using Fe-Mo-MgO (FMMO) as catalyst. This catalyst had an extremely high degree of crystallinity with high porosity. Such high porosity facilitated the rapid growth of nanotubes. Using XRD, Raman spectroscopy, SEM and TEM techniques, the coiled nanotubes were developed in a crystalline consisting of 40 to 60 nm in diameters, coil pitches of 200 to 400 nm and hollow cores of 10 to 15 nm. Raman analysis yielded an I_D/I_G ratio of 0.66, signifying good graphitisation with minimal defect density. Biological evaluations revealed that C-MWCNTs exhibited strong anticancer activity against PA-1 ovarian cancer cells, producing a dose-dependent reduction in cell viability with a well-defined IC_{50} value. Furthermore, the biological analysis showed that C-MWCNTs are highly effective against helminths, causing notable paralysis and death that increased with concentration. These combined biological effects emphasize the synergistic capabilities of these nanomaterials in treating both cancer and parasitic diseases. Thus, it renders that the C-MWCNTs are very useful for specialised applications involving the nanomedicine field, such as treating cancers and parasites.

Keywords: Coiled MWCNTs, FMMO catalyst, Chemical vapour deposition, Anticancer activity, Anthelmintic activity.

INTRODUCTION

Coiled multi-walled carbon nanotubes (C-MWCNTs) form a special category among carbon nanotubes, as a helical structure makes C-MWCNTs more surface-reactive and biologically interactive compared to straight MWCNTs [1,2]. CNTs can be produced using a number of methods and every method has its own advantages and disadvantages related to the yield, crystal nature and scalability. Some popular techniques for the production of CNTs are the arc discharge and laser ablation techniques, where the graphite is ablated at a very high temperature [3]. Such a process yields CNTs that are very crystalline in nature. The techniques mentioned above generally have a low yield rate and are highly costly, hence they are appropriate only for use at the laboratory scale. The HiPco method produces iron nanoparticles that can break down carbon monoxide at high pressure into SWNCTs of smaller diameter and purer form, but this technique requires expensive and advanced equipment [4].

Chemical vapour deposition (CVD) produces carbon-metal MWCNTs *via* catalytic decomposition of hydrocarbons like methane or acetylene. It allows precise control over nanostructure growth [5,6]. The main reason for this helical structure is stress inhomogeneity and differences in lattice structure and a combination of two or more different phases in the catalyst because of the helical arrangement of carbon atoms [7,8].

The morphology of C-MWCNTs, including coil pitch, tube diameter and number of walls, can be finely tuned by controlling growth conditions such as temperature, gas flow, catalyst type and reaction time. Advanced methods like plasma-enhanced CVD and template-assisted techniques further improve the uniformity and crystallinity. Recent developments in CVD have enabled precise control over structural parameters, enhancing their potential in various applications [9-11].

Multi-walled carbon nanotubes with coiled or helical structures differ from straight CNTs due to stress imbalances, asymmetric catalysis and carbon diffusion variations during synthesis. This unique morphology provides higher surface area, defect-rich regions and increased reactivity, making them useful in areas like sensing and energy storage. Despite their promising properties, most of the researches have focused on the straight CNTs, while coiled CNTs remain relatively under-explored. The spiral shape of C-MWCNTs may enhance their interaction with the surfaces of parasitic worms, resulting in membrane damage, reduced nutrient absorption and impeded movement, akin to the mechanisms of conventional anthelmintic drugs [12]. Findings have shown that C-MWCNTs can provoke oxidative stress, hence causing structural injury in helminths, leading to paralysis and eventually death [13]. This makes C-MWCNTs an excellent platform in the development of a novel nanosystem for the treatment of helminthic infections, with the potential for improved drug efficacy and reduced side effects over currently available drugs. The PA-1 line of cells in the ovary is one of the cell types commonly used as a metastatic cell line in the development of aggressive models of ovary cancer, serving as a platform in testing the efficacy of anticancer drugs *in vitro* [14,15]. The testing of C-MWCNTs cytotoxicity on PA-1 cells provides an excellent platform for understanding the cell shape-related biologic activity and the development of multifunctional therapeutic agents.

The increasing focus on animal welfare has encouraged the adoption of organic, free-range and backyard poultry systems, which play an important role in supporting rural livelihoods and nutrition. However, these systems are increasingly threatened by helminth infections, particularly in the tropical regions like India, where chickens and turkeys are highly susceptible. Among these parasites, *Raillietina* species (tapeworms) commonly infect domestic chickens (G*allus gallus domesticus*), causing intestinal inflammation and reduced growth in young birds [16]. Moreover, the effectiveness of widely used anthelmintics such as imidazothiazoles, benzimidazoles and ivermectin is declining due to the growing problem of multi-drug resistance [17]. In this study, C-MWCNTs were synthesised and structurally characterised and their biological activities were systematically evaluated. Special attention was given to their anticancer efficacy against PA-1 ovarian cancer cells, as well as their anthelmintic potential in the context of rising helminth drug resistance. These results collectively underscore the multifunctional biomedical relevance of C-MWCNTs in both cancer treatment and parasite control.

EXPERIMENTAL

All chemicals employed were of AR grade. Iron(III) nitrate hexahydrate, ammonium molybdate tetrahydrate and magnesium nitrate hexahydrate used in the preparation of the Fe-Mo-MgO (FMMO) catalyst were obtained from Merck, India. High-purity gases, including hydrogen (99.99%), nitrogen (99.99%) and C_2H_2, required for the production C-MWCNTs, were supplied by Bharani Enterprises, Chennai, India.

Synthesis of Fe-Mo-MgO (FMMO) catalyst: The FMMO material was synthesised by aqueous combustion synthesis by adopting the reported procedures [2,5]. The stoichiometric amounts of $(NH_4)_6Mo_7O_{24}$, $Fe(NO_3)_3$ and $Mg(NO_3)_2$ were dissolved in distilled water to obtain $Fe_{0.1}Mo_{0.25}MgO_{0.65}$ material. The solution was stirred until all the salts were completely dissolved. Then, 1.5 g of citric acid was added to help the solution foam and burn. The mixture was then placed in a China dish and heated at 550 ºC for 5 min in a high-temperature furnace to start the combustion process. The solid product was subsequently calcined in air at 600-800 ºC to remove residual organic matter and in order to facilitate the development of a well-defined crystalline oxide phase [1].

Growth of coiled multiwalled CNTs: C-MWCNTs were produced through CVD using the FMMO catalyst. To activate the surface of the catalyst, it was put inside a quartz tube furnace and heated to 600 ºC while nitrogen (200 mL/min) and hydrogen (100 mL/min) flowed through it. After that, acetylene gas (20 mL/min) was added as the carbon source, which caused carbon nanotubes to grow on the catalyst particles. The C-MWCNTs were purified by rinsing with deionised water followed by dil. HCl and then dried [18,19].

Collection of *E. eugeniae*: Prior to testing, *E. eugeniae* were collected from moist soil and maintained for several days in cow dung under dark conditions at a constant temperature of 25 ºC. For the experiment, earthworms that were 4 to 6 cm long and 0.2 to 0.3 cm wide were chosen [20].

Evaluation of anthelmintic activity: Mature *Eudrilus* eugeniae worms were evaluated under laboratory conditions to assess their behaviour in the presence of C-MWCNTs. The standard drug was albendazole at a concentration of 100 mg/mL and the control was normal saline. Groups of six similar worms were exposed to each treatment and the time until paralysis and death was noted. Death was confirmed by the lack of movement after shaking the worms or placing them in warm water at 50 ºC [21,22].

Cell line and culture: The PA-1 ovarian cancer cell line was obtained from NCCS, Pune, India and grown in DMEM containing 10% FBS, 100 U/mL penicillin and 100 µg/mL streptomycin, kept at 37 ºC in a humidified environment with 5% CO_2.

***In vitro* assay for anticancer activity (MTT assay):** PA-1 cells (1×10^5/well) were cultured in 24-well plates, treated with samples for 24 h, incubated with MTT (5 mg/mL) for 4 h, dissolved in DMSO and absorbance measured at 570 nm. The IC_{50} values were calculated graphically.

Characterization: XRD patterns of the FMMO catalyst and C-MWCNTs were obtained using a SmartLab (Rigaku, Japan). Morphological and spectral examination was characterised using FESEM Quattro S (FEI Company, Singapore). Energy dispersive X-ray spectroscopy (EDX) provides a quantitative and/or qualitative identification of chemical elements in the entire C-MWCNTs. The structural details of the CNTs were further investigated by HR-TEM (JEOL JEM-2100 Plus, Japan). Raman spectrum was recorded on confocal Raman spectroscopy (Alpha300R). Mature *E. eugeniae* were tested *in vitro* for motility against C-MWCNTs. The cytotoxicity studies were performed in Ovarian cancer cell line PA-1 by using C-MWCNTs samples at different concentrations.

RESULTS AND DISCUSSION

XRD studies: The XRD pattern of the FMMO catalyst exhibited distinct diffraction peaks, confirming the formation of a crystalline mixed oxide phase. Fig. 1 represent the characteristic reflections of FMMO catalyst were observed at 2θ ≈ 26.5º (002), 33.2º (100), 35.7º (111), 43.1º (200) and 62.5º (220), which are indexed to Fe_2O_3 (JCPDS No. 33-0664). Additional peaks at 2θ ≈ 23.3º, 27.3º, 36.2º and 53.5º indicate MgO (JCPDS No. 45-0946), on the other hand minor peaks at 2θ ≈ 23.5º, 25.7º, 27.2º and 47.5º were assigned to MoO_3 phases (JCPDS No. 05-0508). The presence of sharp and intense peaks indicated high crystallinity of the catalyst, whereas the absence of unidentified peaks confirmed phase purity. The crystallite size was calculated (on average) with the help of Scherrer equation for the (101) reflection, was found to be in the nanometer range, suggesting that the catalyst is well-suited for catalytic growth of carbon nanotubes due to its high surface activity.

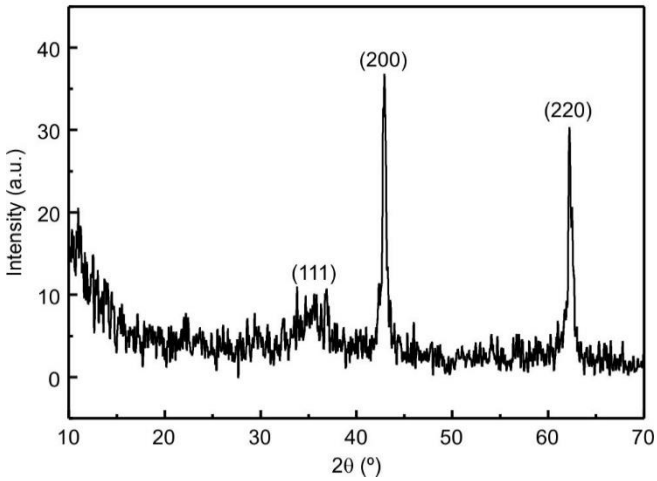

Fig. 1. XRD pattern of FMMO catalyst

The X-ray diffraction (XRD) analysis was also performed to examine the crystallinity and lattice structure of the CNTs, providing insight into their degree of graphitization and structural ordering. The diffraction pattern (Fig. 2) shows two clear peaks at 2θ = 25.88º and 42.85º. These peaks are indexed to the (002) and (100) planes of hexagonal graphite (JCPDS No. 41-1487). The (002) reflection corresponds to the interlayer stacking of graphene sheets along the c-axis, while the (100) peak represents in-plane graphitic ordering. From Bragg's law, the interlayer spacing (d_{002} ≈ 0.344 nm) and in-plane spacing (d_{100} ≈ 0.211 nm) were calculated, values that are typical for multi-walled carbon nanotubes and consistent with their rolled graphitic sheet structure.

The sharpness of these peaks shows that the structure is well-organised and graphitised. Nevertheless, the slight broadening observed in the (002) reflection points to nanoscale phenomena like limited crystallite size, lattice strain and structural curvature, typical of helical or coiled nanotube shapes. This broadening also indicates a small degree of structural disorder caused by the bending of graphitic layers, a characteristic commonly linked to increased surface reactivity [23].

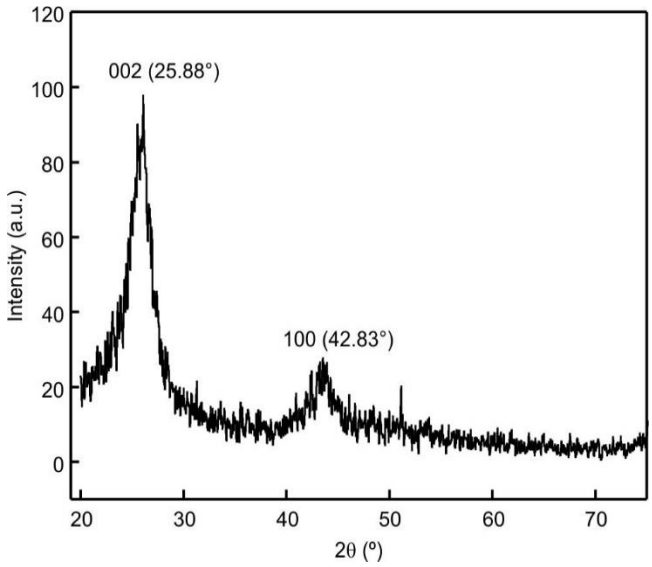

Fig. 2. XRD pattern of coiled MWCNTs

Significantly, no additional reflections corresponding to catalyst residues (such as Fe oxide, Mo oxide or MgO) were observed, confirming the effectiveness of the purification step and indicating the high purity of the obtained CNTs. The lack of additional peaks also implies that only minimal amounts of amorphous carbon are present, as supported by the smooth baseline in the diffraction pattern. While the XRD data revealed a highly crystalline and well-graphitised structure for the produced coiled MWCNTs, the data from Raman spectroscopy demonstrated an I_D/I_G ratio of 0.66; hence, there are slight defects in the crystalline structure linked to their helical shape. Such structural properties associated with good crystallinity, controlled disorder and purity play a very vital role in nanomedicine, catalysis and energy storage since the modification of these properties can change conductivity, stability and surface reactivity.

SEM studies: The surface morphology of the prepared catalyst ($Fe_{0.1}Mo_{0.25}MgO_{0.65}$) was determined using FESEM analysis. As seen from the micrographs (Fig. 3), the structure obtained was porous and spongy, a common occurrence with combustion-synthesised catalysts. This type of irregular particle shape in a loose packing results in a structure characterised by porosity, enhancing the diffusion of gases and increasing the efficiency of the catalyst. Such small nanocrystalline particles with voids between them indicate high surface area, which offers sites for the formation of C-MWCNTs. The porous structure indicates that the combustion technique is effective for synthesizing a catalyst with lower density and enhanced porosity, making it suitable for the catalytic applications. Higher-magnification images reveal individual nanoparticles distributed as surface decorations around the platelet structures.

The SEM image of coiled carbon nanotubes produced with the FMMO catalyst shows a tightly tangled helical structure. The individual tubes have diameters around 40-60 nm, coil pitches between 200-400 nm and lengths reaching several micrometers (Fig. 4). These nanotubes have smooth surfaces, with equal diameters and form tightly bound bundles, which show that they have been grown uniformly and under

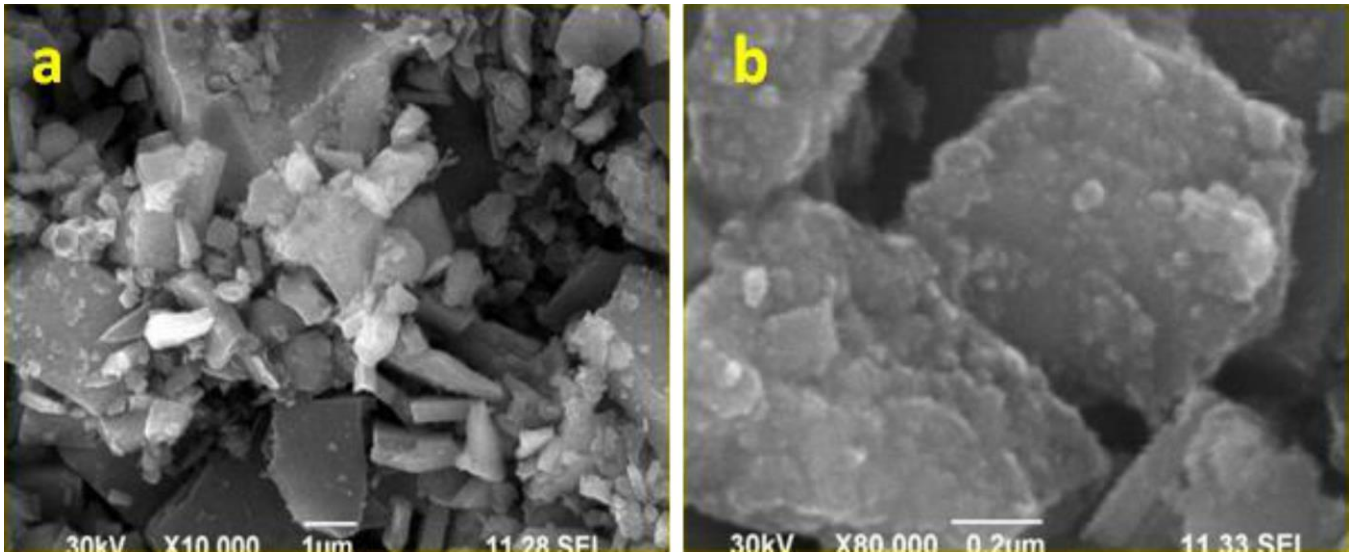

Fig. 3. SEM micrographs of FMMO catalyst showing porous morphology and agglomerated nanoparticles

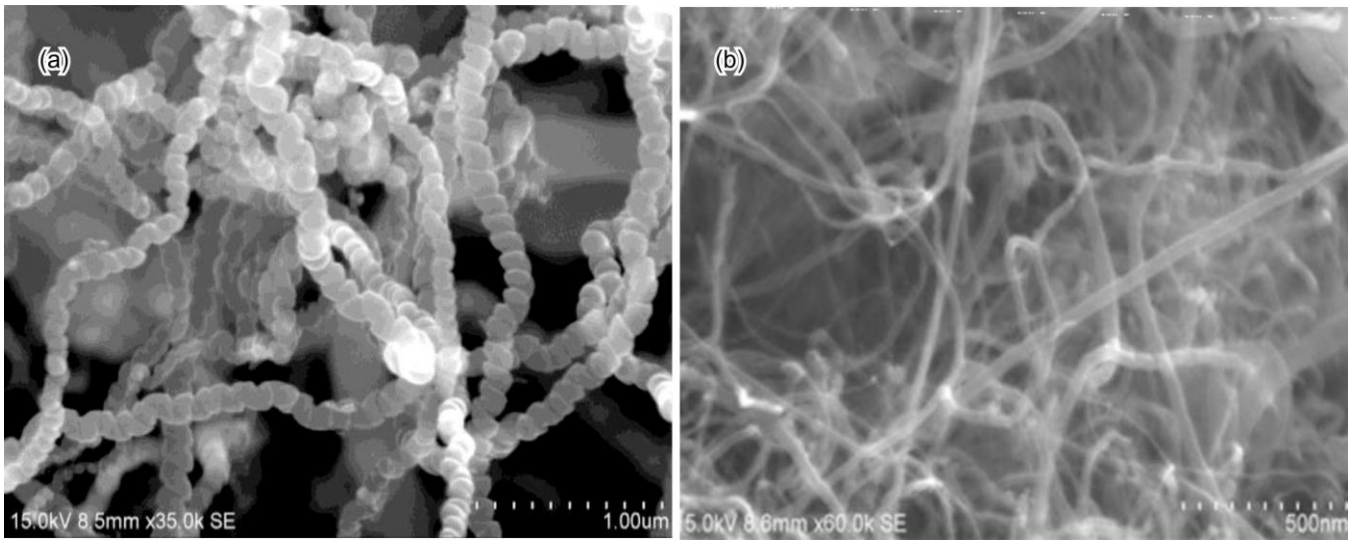

Fig. 4. SEM images of synthesised coiled MWCNTs using FMMO as catalyst

proper control. The defined coiled pattern with very few defects reveals that this material is very strong, which proves that the synthesis process succeeded.

The intertwined helical structure of the CNTs is especially significant since it can boost mechanical strength, increase surface area and enhance interactions with chemical or biological environments. These traits may help cells absorb better and react more quickly on surfaces, making them useful in medicine for things like drug delivery, cancer treatment and fighting parasites. Furthermore, the linked bundles and spiral structure might enhance electron conductivity and provide mechanical strength, indicating their potential use in advanced nanocomposites and catalysts. These results show that the synthesised C-MWCNTs have very strong structures and many useful properties.

EDAX studies: The compositional analysis of the optimised $Fe_{0.1}Mo_{0.25}MgO_{0.65}$ catalyst was observed using EDAX. The spectrum (Fig. 5) shows the peaks corresponding to Fe, Mo, Mg and O. The percentage composition of each element confirming the elements confirms the purity of the sample with no additive impurities in it.

TEM studies: TEM analysis of coiled multiwalled carbon nanotubes revealed clearly defined helical structures composed of multiple concentric graphene layers (Fig. 6a). The nanotubes have hollow cores with inner diameters measuring 10 to 15 nm and outer diameters of 40 to 60 nm. The surfaces of the nanotubes are straight with no defects, which indicates that the nanotubes have strong structures. The entangled nature of the nanotubes indicates that the reason for the curvature might have arisen from the effect of stress on the catalysts or the uneven distribution of carbon in the CVD.

Under higher magnification, Fig. 6b reveals a clearly organised multi-walled structure with clear, regularly positioned concentric graphitic layers and lattice fringes. It manifests crystallinity and graphitisation features. Notably, the bending and twisting do not only widen the surface area but also bend the structure to become more flexible, which might be advantageous for interaction with other molecules and materials.

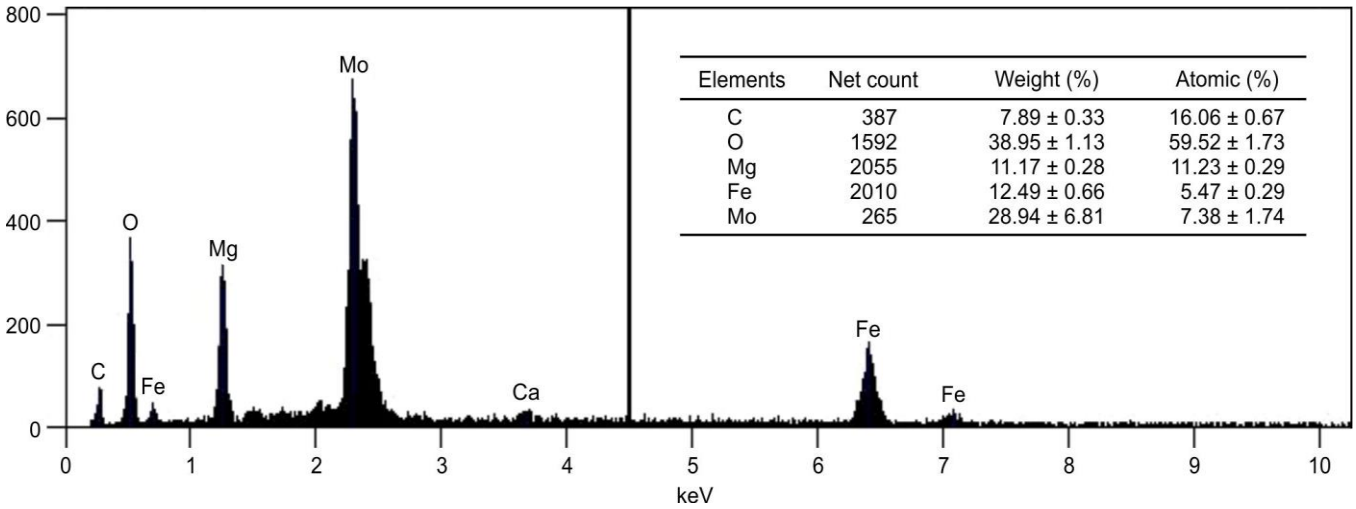

Elements	Net count	Weight (%)	Atomic (%)
C	387	7.89 ± 0.33	16.06 ± 0.67
O	1592	38.95 ± 1.13	59.52 ± 1.73
Mg	2055	11.17 ± 0.28	11.23 ± 0.29
Fe	2010	12.49 ± 0.66	5.47 ± 0.29
Mo	265	28.94 ± 6.81	7.38 ± 1.74

Fig. 5. EDX spectrum of FMMO catalyst

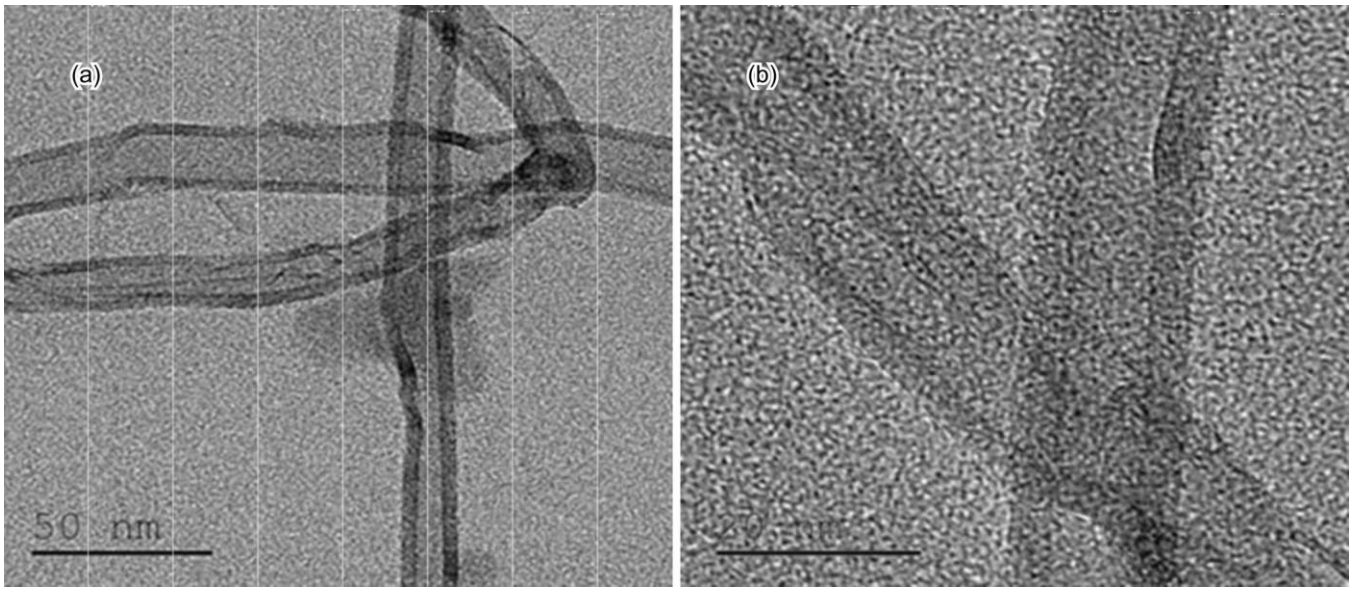

Fig. 6. TEM images of synthesised coiled MWCNTs using FMMO as catalyst

Raman spectral studies: The Raman spectrum of coiled carbon nanotubes (CNTs) produced with the FMMO catalyst displays two main peaks: the D band at 1334.59 cm^{-1}, which indicates defects or structural irregularities and the G band at 1561.28 cm^{-1}, associated with the in-plane vibrations of sp^2-hybridised carbon atoms in graphitic materials (Fig. 7). The measured ID/IG ratio of 0.66 signifies a low level of defects and a high degree of graphitisation, indicating excellent structural quality. This high degree of crystallinity can be attributed to the fact that Fe and Mo species on MgO are used as catalysts in carbon growth, which aids in uniform carbon growth and reduces lattice distortions during chemical vapour deposition. It appears that the helical structure does not affect the architecture of carbon nanotubes, as the ratio of D and G bands is relatively low. This makes sure that the graphitic material is arranged in a very neat way and such materials are very used in several applications such as electronics, nanomedicines, energy storage and catalysis.

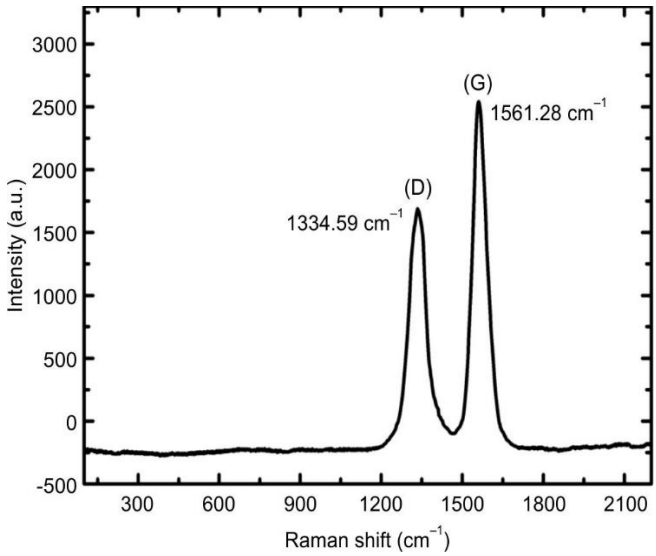

Fig. 7. Raman spectrum of synthesised coiled MWCNTs

***In vitro* anthelmintic activity:** The anthelmintic potency of C-MWCNTs was carried out by infecting *E. eugeniae* worms with six different concentrations: (10, 20, 30, 40, 50 and 60 µL/mL distilled water). The protocol for carrying out *in vitro* experiments has been followed accurately, with particular attention given to recording the time for which worms underwent paralysation and eventually death. The results in Table-1 showed that C-MWCNTs worked quickly at a concentration of 60 µL/mL, causing paralysis in 6 min and death in less time than the standard drug albendazole (100 mg/mL) (Fig. 8). Thus, the distinct nanostructure possessed by C-MWCNTs is highly effective due to its capability of significantly inter-acting with the outer covering and internal mechanism of the worm, thereby disrupting its natural functions. The results suggest that C-MWCNTs possess a remarkable anthelmintic potential compared to the conventional treatment method, especially when used in more concentrated doses.

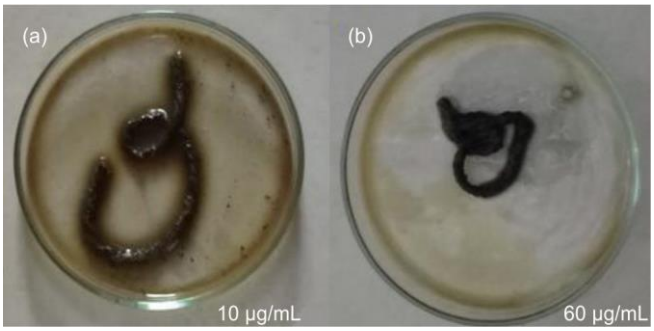

Fig. 8. *In vitro* anthelmintic activity of C-MWCNTs against *E. eugeniae*. (a) shows active worm and (b) at 60 µL/mL concentration shows paralysis and death indicating higher efficacy.

TABLE-1
PARALYSIS AND DEATH TIME DATA OF *E. eugeniae* AT DIFFERENT C-MWCNTs CONCENTRATIONS

Concentration (µL/mL)	Albendazole	C-MWCNTs
10	28	24
20	25	21
30	21	18
40	17	14
50	14	12
60	10	06

Anticancer activity: The cytotoxic potential of C-MWCNTs was assessed on PA-1 ovarian cancer cells using the MTT assay (Table-2). The cells were exposed to C-MWCNTs at doses of 50, 100 and 150 µg/mL for 24 h, resulting in a noticeable concentration-dependent reduction in cell growth. Cell viability decreased from 63.39% at 50 µg/mL to 51.42% at 100 µg/mL, achieving the maximum cytotoxic effect of 21.93% at 150 µg/mL, in contrast to 78% viability in the untreated control cells (Fig. 9).

The notable toxic effect of C-MWCNTs is due to their coiled nanostructure, which improves their uptake by cells and facilitates strong interactions with the cell membrane. Once inside the cell, C-MWCNTs can cause oxidative stress, impair mitochondrial function and trigger apoptosis through caspase signalling pathways. These combined effects result in a dose-dependent inhibition of cancer cell proliferation, highlighting the potential of C-MWCNTs as effective and targeted nanomaterials for anticancer therapy [24-26].

TABLE-2
CYTOTOXIC ACTIVITY DATA OF SYNTHESISED COILED MWCNTS ON PA-1 OVARIAN CANCER CELLS

Concentration (µg/mL)	Absorbance (O.D.)	Cell viability (%)
150	0.154	21.93 ± 0.650
100	0.361	51.42 ± 0.720
50	0.445	63.39 ± 0.840
Cell control	0.702	78.16 ± 2.954

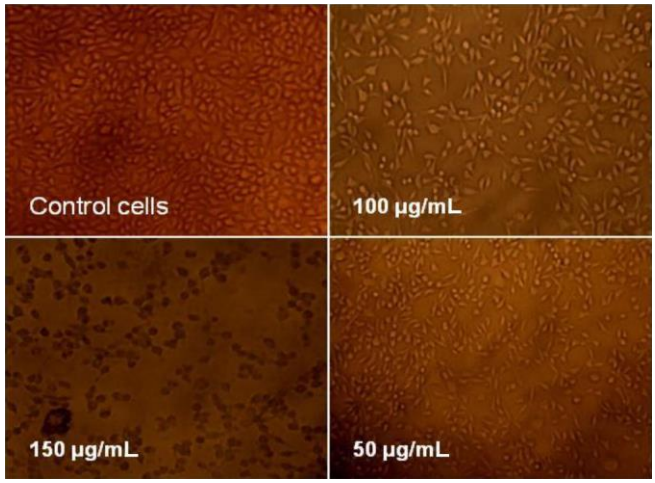

Fig. 9. Cytotoxic effect of C-MWCNTs on PA-1 ovarian cancer cells showing concentration-dependent reduction in cell viability at 50, 100 and 150 µg/mL compared to control after 24 h treatment.

Conclusion

Coiled multiwalled carbon nanotubes (C-MWCNTs) were prepared using an Fe-Mo-MgO catalyst through chemical vapour deposition (CVD) and found to have a well-defined helical structure with high crystallinity. The characterisation results confirmed their excellent graphitisation and high purity. The *in vitro* studies demonstrated that C-MWCNTs exhibit pronounced cytotoxicity toward PA-1 ovarian cancer cells in a concentration-dependent manner. A significant reduction in cell viability was observed, with a well-defined IC_{50} value. The distinctive coiled morphology likely enhances the surface activity and cellular interactions, thereby contributing to improved anticancer efficacy. Along with being toxic to cells, C-MWCNTs were also very effective against *E. eugeniae*. The worms quickly became paralysed and died when the dose was higher. The highest dose (60 µL/mL) caused full paralysis in just 6 min, which was more effective than the standard drug albendazole. These results suggest that C-MWCNTs are versatile bioactive nanomaterials with potential uses in the cancer treatment as well as anthelmintic therapy, emphasizing the importance of further research into their mechanisms and *in vivo* testing.

CONFLICT OF INTEREST

The authors declare that there is no conflict of interests regarding the publication of this article.

DECLARATION OF AI-ASSISTED TECHNOLOGIES

During the preparation of this manuscript, the authors used an AI-assisted tool(s) to improve the language. The authors reviewed and edited the content and take full responsibility for the published work.

REFERENCES

1. K.T. Lau, M. Lu and D. Hui, *Composites B Eng.*, **37**, 437 (2006); https://doi.org/10.1016/j.compositesb.2006.02.008
2. A. Kumar, R.K. Singh and P. Sharma, *J. Nanobiotechnol.*, **21**, 112 (2023); https://doi.org/10.1186/s12951-023-01845-7
3. N.M. Mubarak, E.C. Abdullah, N.S. Jayakumar and J.N. Sahu, *J. Ind. Eng. Chem.*, **20**, 1186 (2014); https://doi.org/10.1016/j.jiec.2013.09.001
4. V.S. Shenoy Gangoli, M.A. Godwin, G. Reddy, R.K. Bradley and A.R. Barron, *Carbon*, **5**, 65 (2019); https://doi.org/10.3390/c5040065
5. H.J. Dai, *Acc. Chem. Res.*, **35**, 1035 (2002); https://doi.org/10.1021/ar0101640
6. S. Iijima and T. Ichihashi, *Nature*, **363**, 603 (1993); https://doi.org/10.1038/363603a0
7. S. Amelinckx, A. Lucas and P. Lambin, *Rep. Prog. Phys.*, **62**, 1471 (1999); https://doi.org/10.1088/0034-4885/62/11/201
8. S. Zhang, L. Kang, X. Wang, L. Tong, L. Yang, Z. Wang, K. Qi, S. Deng, Q. Li, X. Bai, F. Ding and J. Zhang, *Nature*, **543**, 234 (2017); https://doi.org/10.1038/nature21051
9. T. Saba, K.S.K. Saad and A.B. Rashid, *Heliyon*, **10**, e37976 (2024); https://doi.org/10.1016/j.heliyon.2024.e37976
10. M. Sivakumar and S. Ratchahat, *J. Anal. Appl. Pyrolysis*, **189**, 107093 (2025); https://doi.org/10.1016/j.jaap.2025.107093
11. Z. Chu, B. Xu and J. Liang, *Nanomaterials*, **13**, 2791 (2023); https://doi.org/10.3390/nano13202791
12. X.P. Zhang, W.X. Li, T.S. Ai, H. Zou, S.G. Wu and G.T. Wang, *Aquaculture*, **420-421**, 302 (2014); https://doi.org/10.1016/j.aquaculture.2013.09.022
13. S. Zegbi, F. Sagües, C. Saumell, L. Ceballos, P. Domínguez, I. Guerrero, M. Junco, L. Iglesias and S. Fernández, *Ruminants*, **4**, 10 (2024); https://doi.org/10.3390/ruminants4010002
14. J.N. Nikhitha, K.S. Swathy and R.P. Chandran, *J. Genet. Eng. Biotechnol.*, **19**, 116 (2021); https://doi.org/10.1186/s43141-021-00215-1
15. C. Xiong, B. Yan, S. Xia, F. Yu, J. Zhao and H. Bai, *Saudi J. Biol. Sci.*, **28**, 4900 (2021); https://doi.org/10.1016/j.sjbs.2021.06.033
16. F.A.S. Anwar, N.A. Alkenani, S.K. Abd-Elghaffar, H.E.-D.M. Omar, F.M. Abdel-maksoud, N. Abdelsater, I.S.E. Mohamed, H. Rudayni, M. Al-Zharani, K.M. Dossouvi, A. Elkelish and S.A.A. Mohamed, *Sci. Rep.*, **16**, 43187 (2026); https://doi.org/10.1038/s41598-026-43187-3
17. W. Fissiha and M.Z. Kinde, *Infect. Drug Resist.*, **14**, 5403 (2021); https://doi.org/10.2147/IDR.S332378
18. T. Somanathan and A. Pandurangan, *Nano-Micro Lett.*, **2**, 204 (2010); https://doi.org/10.1007/BF03353642
19. T.N. Suresh and T. Somanathan, *Mater. Today Proc.*, **46**, 4187 (2021); https://doi.org/10.1016/j.matpr.2021.02.755
20. A. Rehman, R. Ullah, I. Uddin, I. Zia, L. Rehman and S.M.A. Abidi, *Exp. Parasitol.*, **198**, 95 (2019); https://doi.org/10.1016/j.exppara.2019.02.005
21. D.G. Kumar, R.R. Achar, J.R. Kumar, G. Amala, V.K. Gopalakrishnan, S. Pradeep, A.A. Shati, M.Y. Alfaifi, S.E.I. Elbehairi, E. Silina, V. Stupin, N. Manturova, C. Shivamallu and S.P. Kollur, *BMC Complement. Med. Ther.*, **23**, 167 (2023); https://doi.org/10.1186/s12906-023-03982-1
22. A.M. Kaiaty, F.A. Salib, S.M. El-Gameel, E.S. Abdel Massieh, A.M. Hussien and M.S. Kamel, *Trop. Anim. Health Prod.*, **55**, 317 (2023); https://doi.org/10.1007/s11250-023-03722-0
23. K.T. Lau, M. Lu and D. Hui, *Composite B Eng.*, **37**, 437 (2006); https://doi.org/10.1016/j.compositesb.2006.02.008
24. I.L. Su, Y.P. Chen, L.C. Hsu, C.W. Feng, K.H. Tsui, N.F. Chen, P.J. Sung, H.M. Kuo and Z.H. Wen, *Eur. J. Pharmacol.*, **1005**, 178070 (2025); https://doi.org/10.1016/j.ejphar.2025.178070
25. D. Zhang, L. Wang, L. Tian, W. Chen, A.F. El-kott, W. Eltantawy, S. Negm and M.O. Alshaharni, *J. Sci. Adv. Mater. Devices*, **9**, 100714 (2024); https://doi.org/10.1016/j.jsamd.2024.100714
26. X. Zhang, B. Xiong, Y. Cheng, J. Huang, J. Xue, X. Li, W. Lu, J. Zhu, L. Wang, W. Yang and Z. Cheng, *Transl. Oncol.*, **56**, 102380 (2025); https://doi.org/10.1016/j.tranon.2025.102380